BRAIN
ORIGINAL ARTICLE

Brain region-specific synaptic function of FUS underlies the FTLD-linked behavioural disinhibition

Jun-Ying Wang,[1,2] Guo-Ming Ma,[1,2] Xiao-Qiang Tang,[1] Qi-Li Shi,[1] Ming-Can Yu,[1] Min-Min Lou,[1,2] Kai-Wen He[1] and Wen-Yuan Wang[1,3,4]

Synaptic dysfunction is one of the earliest pathological processes that contribute to the development of many neurological disorders, including Alzheimer's disease and frontotemporal lobar degeneration. However, the synaptic function of many disease-causative genes and their contribution to the pathogenesis of the related diseases remain unclear. In this study, we investigated the synaptic role of fused in sarcoma, an RNA-binding protein linked to frontotemporal lobar degeneration and amyotrophic lateral sclerosis, and its potential pathological role in frontotemporal lobar degeneration using pyramidal neuron-specific conditional knockout mice (Fus^{cKO}). We found that FUS regulates the expression of many genes associated with synaptic function in a hippocampal subregion-specific manner, concomitant with the frontotemporal lobar degeneration-linked behavioural disinhibition. Electrophysiological study and molecular pathway analyses further reveal that fused in sarcoma differentially regulates synaptic and neuronal properties in the ventral hippocampus and medial prefrontal cortex, respectively. Moreover, fused in sarcoma selectively modulates the ventral hippocampus–prefrontal cortex projection, which is known to mediate the anxiety-like behaviour. Our findings unveil the brain region- and synapse-specific role of fused in sarcoma, whose impairment might lead to the emotional symptoms associated with frontotemporal lobar degeneration.

1 Interdisciplinary Research Center on Biology and Chemistry, Shanghai Institute of Organic Chemistry, Chinese Academy of Science, Shanghai 201210, China
2 University of Chinese Academy of Sciences, Beijing 100049, China
3 Department of Rehabilitation Medicine, Huashan Hospital, Fudan University, Shanghai 200040, China
4 Animal Center of Zoology, Institute of Neuroscience, Kunming Medical University, Kunming 650500, China

Correspondence to: Dr Wen-Yuan Wang
Interdisciplinary Research Center on Biology and Chemistry
Shanghai Institute of Organic Chemistry, Chinese Academy of Science
Bldg. 13, No. 100 Haike Rd, Pudong District, Shanghai 201210, China
E-mail: wywang@sioc.ac.cn

Correspondence may also be addressed to: Dr Kai-Wen He
Interdisciplinary Research Center on Biology and Chemistry
Shanghai Institute of Organic Chemistry, Chinese Academy of Science
Bldg. 13, No. 100 Haike Rd, Pudong District, Shanghai 201210, China
E-mail: kwhe@sioc.ac.cn

Keywords: FTLD; FUS; mPFC; vHPC; synaptic transmission

Received December 01, 2021. Revised August 10, 2022. Accepted September 19, 2022. Advance access publication November 8, 2022

Introduction

Fused in sarcoma (FUS) is an RNA-binding protein widely expressed in the CNS. It is a significant disease gene associated with amyotrophic lateral sclerosis (ALS) and frontotemporal lobar degeneration (FTLD).[1–5] While the molecular mechanism of FUS proteinopathy in ALS was extensively studied in the past several years, the role of FUS in the pathogenesis of FTLD has remained largely unknown. FTLD is one of the most common early-onset dementia that affects behaviour and emotion.[6] About 9% of all FTLD patients show FUS pathology (FTLD-FUS),[7] with severe disinhibition behaviour and, in some cases, with other psychiatric abnormalities but without motor or linguistic deficits.[6] In the brain sections of FTLD-FUS, FUS-immunoreactive neuronal cytoplasmic inclusions were found in the hippocampal pyramidal layer, frontal cortex, striatum etc.,[8] implying that the loss of FUS' function in these brain regions might directly contribute to the disease.

Previous studies have shown that FUS regulates the morphogenesis of dendrites and spines during early development.[9–15] Overexpression of mutant FUS in both zebrafish[16] and *Drosophila*[17] impaired neuromuscular synaptic transmission. In the mammalian brain, a recent study demonstrated that FUS regulates synaptic transmission in the dorsal hippocampus (HPC).[18] Collectively, these studies suggest that FUS is involved in the regulation of synaptic functions.

In this study, we generated pyramidal neuron-specific *Fus* conditional knockout (Fus^{cKO}) mice to investigate the role of FUS in the adult brain. Transcriptome analysis indicates that the FUS-regulated genes were strongly involved in synaptic function with hippocampal sub-region specificity. Interestingly, we recorded hippocampal pyramidal neurons of Fus^{cKO} mice and found that the intermediate HPC (iHPC) showed enhancement, while the ventral HPC (vHPC) displayed reduction in excitatory synaptic transmission. The region specificity was also observed between the vHPC and the medial prefrontal cortex (mPFC), both highly associated with the FTLD-linked behavioural disinhibition.[19–21] The spike frequency adaptation decreased in vHPC pyramidal neurons, while increased in mPFC pyramidal neurons due to the FUS deletion. We further identified the selective enhancement of synaptic transmission from vHPC to mPFC in the Fus^{cKO} mice, which might be directly related to disruptive avoidance behaviour. Furthermore, we found the deletion of FUS reduced expression of presynaptic genes in vHPC, while decreased expression of postsynaptic genes in mPFC, providing a potential molecular mechanism for FUS' region-specific regulation. Our findings revealed the brain region- and synapse-specific role of FUS and the potential contribution of dysfunctional FUS to the FTLD-linked behavioural disinhibition.

Materials and methods

Animals

All procedures were approved by the Institutional Animal Care and Use Committees at the Interdisciplinary Research Center on Biology and Chemistry, Chinese Academy of Science. All mice were housed on a 12 h light/12 h dark cycle with food and water *ad libitum*. The Cre-loxP system was used for conditional *Fus* knockout mice generation. The same directional loxP sites were inserted into the intron 3–4 and intron 6–7 of the *Fus* gene by the CRISPR–Cas9 system to obtain $Fus^{fl/fl}$ mice. We crossed $Fus^{fl/fl}$ mice with Camk2α-Cre mice (Shanghai Model Organisms, Shanghai, China) or Nestin-Cre mice (Model Animal Research Center of Nanjing University, Nanjing, China) to generate conditional *Fus* knockout mice. The Nestin-Cre; $Fus^{fl/fl}$ mice and Nestin-Cre mice were only used for RNA sequencing. For other experiments, Camk2α-Cre and $Fus^{fl/fl}$ were used as controls, Camk2α-Cre; $Fus^{fl/fl}$ mice were used as Fus^{cKO} experimental mice. Adult male mice (2–3 months old) were used for all experiments.

RNA sequencing

Male Nestin-Cre and Nestin-Cre; $Fus^{fl/fl}$ mice (2-month-old) were deeply anaesthetized with isoflurane, the HPC was removed and divided into dorsal HPC (dHPC), iHPC and vHPC as shown in Fig. 1A. Total RNA was extracted using TRIzol™ (Thermo Fisher Scientific) following the manufacturer's instructions. The concentration and purity of the RNA samples obtained were quantified by NanoDrop 2000c spectrophotometer (Thermo Fisher Scientific). RNA sequencing (RNA-seq) was performed using HiSeq2000 Sequencing System (Illumina).

For RNA-seq analysis, three biological replicates were used for each experimental group. Two samples were identified as outliers via principal components analysis and were removed from further analysis. Adapters of raw sequencing reads obtained from RNA-seq were removed using Cutadapt (v.2.8).[22] Cleaned reads were mapped to the reference mouse genome (GRCm38/mm10) using HISAT2 (v.2.1.0)[23] with default parameters. Reads were then quantified via feature Counts (v.1.6.2).[24] The annotation GTF file was downloaded from Ensembl (v.GRCh38.93).

We performed unsupervised hierarchical clustering using the hclust function in R based on the sample distances. Genes were analysed for differential expression using R package DESeq2 (v.1.24.0).[25] The Benjamini and Hochberg procedure was applied to adjust for multiple hypothesis testing, and differential expression gene candidates were selected with a false discovery rate <0.05. Gene Ontology analysis of differentially expressed genes with gene symbols was performed using MetaScape.[26]

Western blotting

The mPFC tissues were collected and transferred into the lysis buffer containing 50 mM Tris (pH 7.5), 150 mM NaCl, 1% NP-40, 0.5% sodium deoxycholate and 0.1% sodium dodecyl-sulphate (SDS) supplemented with 1× phenylmethylsulphonyl fluoride (Beyotime). Samples were kept on ice and homogenized by the Homogenizer WorkCentre (IKA, T10). The lysates were incubated on ice for 10 min and centrifuged at 14 000*g* at 4°C for 15 min and the supernatants were collected for SDS–polyacrylamide gel electrophoresis (SDS–PAGE). The proteins were separated by SDS–PAGE, transferred onto a polyvinyl difluoride membrane and then blocked with 5% (m/v) non-fat milk for 1.5 hours at room temperature. The following primary antibodies were used: mouse anti-FUS (1:1000, sc-47711, Santa Cruz Biotechnology) and rabbit anti-α-Tubulin (1:40 000, PM054, MBL Beijing Biotech). Secondary antibodies conjugated to horseradish peroxidase against mouse or rabbit IgG were obtained from Jackson ImmunoResearch Laboratories (1:10 000). The visualization was performed via Fusion SoloS. EDGE V0.70 (Vilber Lourmat), and the Evolution-Capt software (Vilber Lourmat) was used for quantification.

Immunofluorescence

Mice were deeply anaesthetized with isoflurane and transcardially perfused with 10 ml of 1× phosphate buffered saline (PBS) and fixed with 40 ml of 4% paraformaldehyde (PFA) in sodium phosphate buffer (pH 7.4). The brains were post-fixed overnight in 4% PFA at 4°C

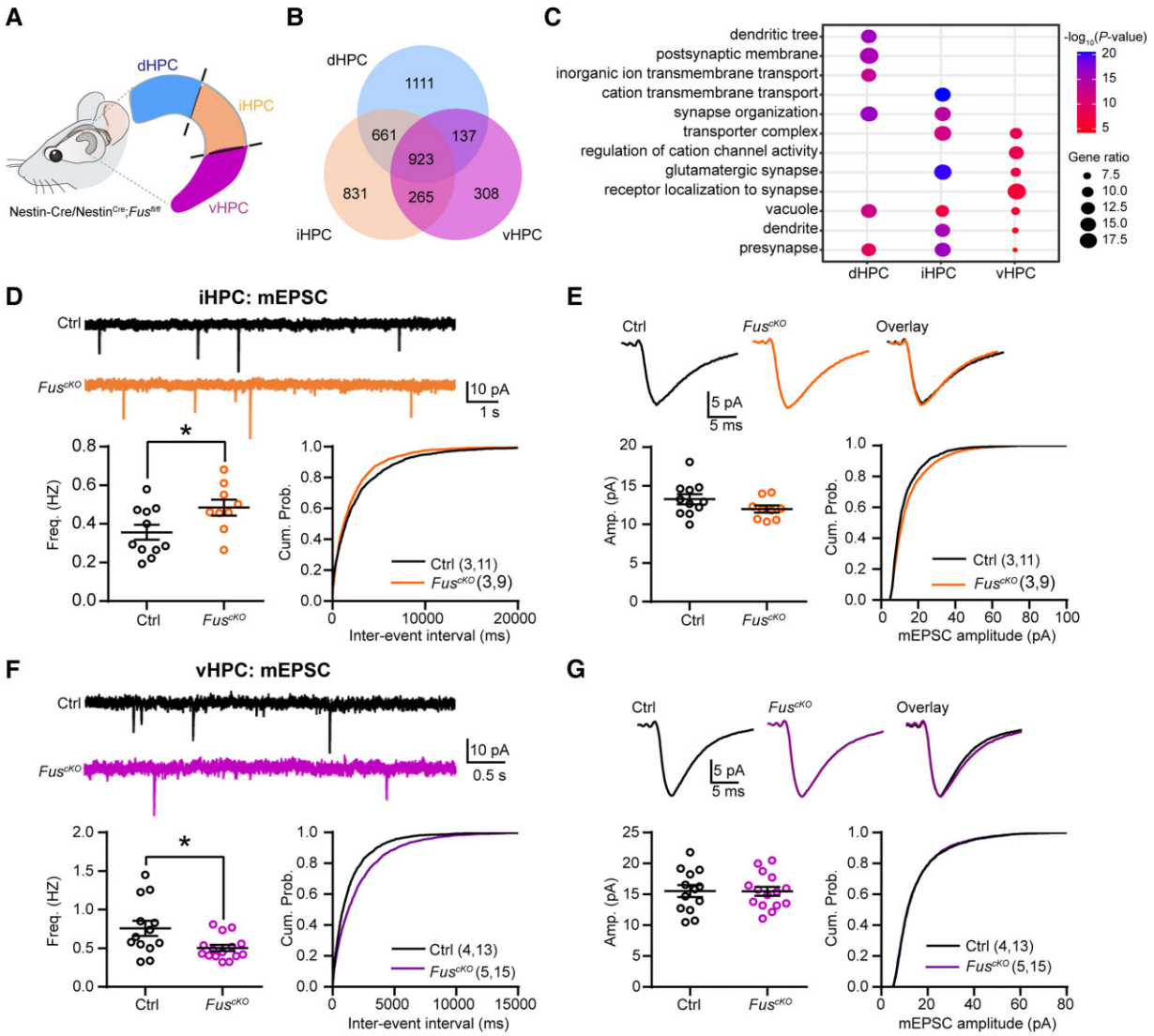

Figure 1 Hippocampal subregion-specific roles of FUS in gene expression and synaptic transmission. (**A**) A diagram illustrating the dissection strategy of the dHPC, iHPC and vHPC used in this study. (**B**) Venn diagram illustrating DEG between dHPC, vHPC and iHPC in Ctrl or Fus^{cKO} mice. (**C**) Dot plot showing top enriched GO terms for FUS knock out specific downregulated genes in dHPC, iHPC and vHPC. (**D**) Miniature excitatory postsynaptic current (mEPSC) frequency of iHPC pyramidal neurons was higher in Fus^{cKO} mice compared with Ctrl mice. *Top*: Representative traces of mEPSC at iHPC pyramidal neurons in Ctrl and Fus^{cKO} mice. *Bottom left*: Summary of mEPSC frequency in iHPC pyramidal neurons. Student's *t*-test; $^{*}P = 0.04$. *Bottom right*: There was a leftwards shift in the cumulative probability histogram of the inter-event intervals at Fus^{cKO}. Kolmogorov–Smirnov (KS); $P < 0.0001$. (**E**) mEPSC amplitude and kinetics of iHPC pyramidal neurons did not differ between Ctrl and Fus^{cKO} mice. *Top*: Average traces of well-isolated events. *Bottom left*: Summary of mEPSC amplitude in iHPC pyramidal neurons. Student's *t*-test; $P = 0.15$. *Bottom right*: The distribution of individual event amplitudes was different between groups. KS; $P < 0.0001$. (**F**) mEPSC frequency of vHPC pyramidal neurons was lower in Fus^{cKO} mice compared with Ctrl mice. *Top*: Representative traces of mEPSC at vHPC pyramidal neurons in Ctrl and Fus^{cKO} mice. *Bottom left*: Summary of mEPSC frequency in vHPC pyramidal neurons. Student's *t*-test; $^{*}P = 0.02$. *Bottom right*: There was a rightwards shift in the cumulative probability histogram of the inter-event intervals at Fus^{cKO}. KS; $P < 0.0001$. (**G**) mEPSC amplitude and kinetics of vHPC pyramidal neurons did not differ between Ctrl and Fus^{cKO} mice. *Top*: Average traces of well-isolated events. *Bottom right*: Summary of mEPSC amplitude in vHPC pyramidal neurons. Student's *t*-test; $P = 0.97$. The distribution of individual event amplitudes was comparable between groups. KS; $P = 0.33$. Sample size indicated as (mice, cells). Data are presented as the mean ± SEM.

and then were sectioned into 50-μm-thick coronal slices with a vibratome (Leica VT 1000S). The slices were incubated in 0.05% Triton X-100 in PBS for 30 min and blocked-in blocking media (5% normal goat serum, 0.3% Triton X-100 in PBS) for 2 h at room temperature. Then slices were incubated with rabbit anti-FUS antibodies (1:500, A300–302A, Bethyl Laboratories) and chicken NeuN (1:5000, ABN91, Millipore) in 2% normal goat serum and 0.1% Triton X-100 overnight at 4°C. After being washed with PBS, slices were incubated in the secondary antibodies conjugated with 647 (1:500, anti-rabbit IgG, 111-605-003, Jackson ImmunoResearch Laboratories) and 568 (1:1000, anti-chicken IgG, A-11041, Invitrogen) for 1.5 h at room temperature. After being air-dried, slices were cover-slipped with a Mounting medium (Prolong gold antifade reagent, Invitrogen). Images were recorded on a spinning disc microscope (Andor Technology).

Behavioural assays

Behavioural assays were performed during the light cycle. All the experimental mice were transferred to the testing room at least

30 min before the tests. Mice were examined in open field test, elevated-plus maze test, Y-maze test, Barnes maze test and social interaction test. The apparatus was completely cleaned with 70% alcohol and air-dried between testing of each mouse. Mice were used for each behavioural test only once.

Open field test

Mice were placed in the centre of the open field test chamber (40 × 40 cm) and allowed to explore for 10 min freely. The luminance inside the chamber was kept at ~35 lumen (lx). Mice activity was measured automatically by the EthoVision XT (Noldus11.5, Noldus Information Technologies, NED). The open field was divided into a centre zone (20 × 20 cm) and a surrounding zone. Measurements included distance and time spent in the centre zone.

Elevated-plus maze test

The elevated-plus maze device consists of two open arms (36 × 5 × 0.3 cm) and two closed arms (36 × 5 × 18 cm). Mice were placed on the centre (5 × 5 cm) of the device and allowed to explore for 5 min in each trail. The device was elevated to 45 cm above the floor, and the luminance was kept at ~35 lx. The duration of time spent in open arms and the count of arm entries was measured using SMART software (Panlab).

Y-maze spontaneous alternation test

The Y-maze consists of three connected arms (30 × 6 × 15 cm) at 120° angles from each other. Mice were placed on one arm of the Y-maze and allowed to freely explore for 10 minutes under light with a luminance of ~35 lx. The number of entries and spontaneous alternations were measured and calculated using EthoVision XT (Noldus11.5).

Barnes maze test

The Barnes maze apparatus includes a white circular platform (diameter = 90 cm) containing 20 equally spaced holes (diameter = 5 cm), a start chamber and an escape tunnel mounted under any of the 20 escape holes. The device was elevated to 60 cm above floor, and the luminance was kept at ~300 lx. Visual cues were inserted in the wall around the Barnes maze. Mice were transported to the centre of the platform via the start chamber where they remained for 30 s before the 3 min of exploring under 90 dB of white noise. The latency was the time needed to find the target hole. Two trials per day were conducted for six successive days. Probe trail was performed on Day 7 without the escape tunnel. The time spent in the target quadrant was recorded and analysed using EthoVision XT (Noldus11.5).

Three-chamber social interaction test

The apparatus was composed of three chambers (40 × 20 × 23 cm), connected by two openings (10 × 23 cm) in the middle, allowing the mice free movement. Two plastic cages were placed in the middle of the left and right chambers. The experiment was divided into three stages. In the first stage, the subject mouse was placed in the middle chamber, and then the baffles on both sides were removed so the mice could move freely for 10 minutes. At the second stage, one stranger mouse was placed in the cage in one of the side chambers. Then the subject mice were allowed to explore for 10 min. At the third stage, another stranger mouse was placed in the empty cage and the subject mouse was allowed to freely explore for 10 min. The time spent in each chamber and the area near the plastic cages, and the count of each chamber entries were measured using EthoVision XT (Noldus11.5).

Virus injection

The 4–6-week-old mice were bilaterally injected with AAV2/9-hEF1a-DIO-hChR2(H134R)-EYFP (adeno-associated viral vector serotype 2/9) virus (Shanghai Taitool Bioscience Company, China) into the vCA1 under isoflurane anaesthesia. In each hemisphere, 150 nl of 10^{12} vg/ml virus was pressure-injected using a glass micropipette at a rate of 20 nl/min. The injection site coordinates (posterior to bregma, anterioposterior; lateral to the midline; below the bregma, dorsoventral; in millimetres) were anterioposterior −3.39, midline ± 3.60, dorsoventral −3.60. After injection, mice recovered for >6 weeks before electrophysiological experiments.

Electrophysiological recordings

Here, 300-μm-thick coronal slices containing mPFC, or transverse sections of the HPC were cut in ice-cold dissection buffer containing 212.7 mM sucrose, 5 mM KCl, 1.25 mM NaH_2PO_4, 10 mM $MgCl_2$, 0.5 mM $CaCl_2$, 26 mM $NaHCO_3$ and 10 mM dextrose with 95% O_2 and 5% CO_2. Then slices were transferred to normal artificial CSF (ACSF) containing 119 mM NaCl, 5 mM KCl, 1.25 mM NaH_2PO_4, 2 mM $CaCl_2$ and 1 mM $MgCl_2$, and incubated at 30°C for 30 min. Slices were then transferred to room temperature incubate for at least 30 min before whole-cell recording.

For whole-cell recordings, pyramidal neurons in the HPC or mPFC were patched under infrared differential interference contrast microscopy (OLYMPUS). The glass pipette recording electrodes had open tip resistances of 4–6 MΩ and were filled with different internal solutions (pH 7.2–7.3, 280–295 mOsm) according to each assay. Pyramidal neurons with an input resistance of >100 MΩ and access resistance of <25 MΩ were recorded. Data were sampled at 10 kHz and filtered to 2 kHz by MultiClamp 700B (Molecular Devices) and Axon™ Digidata® 1550B (Molecular Devices). Recordings were analysed using Clampfit (Molecular Devices) and Mini Analysis Program (Synaptosoft).

Miniature excitatory postsynaptic currents

To isolate AMPAR-mediated miniature excitatory postsynaptic currents (mEPSCs), ACSF with 1 μM TTX, 100 μM D-APV (DL-2-amino-5-phosphonovalerate) and 10 μM gabazine was used. The internal pipette solution contained 125 mM CsOH, 125 mM gluconate acid, 8 mM KCl, 10 mM HEPES, 1 mM EGTA, 4 mM Mg·ATP, 0.5 mM Na_3GTP, 10 mM Na-phosphocreatine and 5 mM QX-314. The membrane potential was held at −60 mV.

Paired-pulse ratio

The paired-pulse responses were evoked with a concentric bipolar microelectrode (FHC) placed in Schaffer collateral inputs from CA3 of the vHPC. The internal pipette solution contained 130 mM K-gluconate, 10 mM KCl, 10 mM HEPES, 0.2 mM EGTA, 4 mM Mg·ATP, 0.5 mM Na_3GTP, 10 mM Na-phosphocreatine and the membrane potential was held at −60 mV. The paired stimulations were current-controlled by the isolated current source (Cygnus) and the inter-stimulus interval was set at 20, 50 or 100 ms. The paired-pulse ratio (PPR) was calculated as the ratio of the second pulse amplitude to that of the first pulse.

Neuronal-firing properties

To measure neuronal-firing properties, whole-cell recording was switched to current-clamped with K^+-based internal solution same as PPR. A 1-s ramp test with injected current from 0–1000 pA was conducted to estimate the spiking threshold of membrane potential and minimal injected current. The frequency–current (*f–I*) relationships were estimated from responses to a series of injected current steps (–50 to 950 pA, in 50 pA increments, 1 s duration).

Light-evoked EPSCs and AMPAR/NMDAR ratio

The ChR2-expressing axon terminals of vCA1 were activated by 470-nm, 5-ms light pulses with a light-emitting diode (LED). The light-evoked EPSCs of mPFC pyramidal neurons were recorded in the presence of 1 μM TTX to block the disynaptic inputs from surrounding neurons, and 10 μM gabazine. The internal solution was caesium hydroxide-based, the same as for the mEPSCs recording, additionally including biocytin (0.1% w/v) for *post hoc* neuron identification. AMPAR/NMDAR ratio was calculated as the ratio of peak EPSC recorded at –60 mV (AMPAR EPSC) to the EPSC recorded at +40 mV, 3× the decay time later than AMPAR EPSC peak time (NMDAR EPSC).

Light-evoked Sr^{2+}-mEPSCs

Modified ACSF was used for Sr^{2+}-mEPSCs recording, containing 4 mM $MgCl_2$ and 4 mM $SrCl_2$ with 0 mM $CaCl_2$. After incubation at 30°C, the slices were transferred to modified ACSF and incubated for at least 30 min before recording. AMPAR-mediated mEPSCs were isolated by adding 1 μM TTX, 100 μM D-APV and 10 μM gabazine to the modified ACSF. Internal pipette solution was the same as the mEPSCs recording. Cells were held at –60 mV, 2 s a sweep with a 10-s interval repeated for 60 replicates were recorded. A 600-ms window before the LED illumination was defined as baseline (pre-LED), and a 600-ms window after a 50-ms delay from LED offset was defined as light-evoked desynchronized events (post-LED). The light-evoked Sr^{2+}-mEPSC was calculated by the following equation:

$$\frac{(A_{post} \times F_{post}) - (A_{pre} \times F_{pre})}{(F_{post} - F_{pre})} \quad (1)$$

A_{post} and F_{post} represent the average amplitude and average frequency of post-LED, and at the same time, A_{pre} and F_{pre} represent the average amplitude and average frequency pre-LED, respectively.

NMDAR-mediated EPSCs

For NMDAR EPSC recording, Mg^{2+}-free ACSF with 4 mM $CaCl_2$ was used, and recordings were performed in the presence of 1 μM TTX, 20 μM CNQX and 10 μM gabazine. Cells were held at –60 mV, and the internal pipette solution was the same as the mEPSCs recording. NMDAR-mediated EPSCs were analysed by calculating the unit charge (nA/s) using MATLAB (MathWorks) scripts (https://github.com/WJY-FUS/NMDA-charge).

Cross-linking immunoprecipitation and high-throughput sequencing

The cross-linking immunoprecipitation and high-throughput sequencing (HITS-CLIP) experiment was performed as described[27] with modifications. Briefly, primary cortical neurons were collected from embryonic day 16 pups. Neurons 9 days *in vitro* were soaked in ice-cold PBS buffer and then irradiated with an ultraviolet ray (UV) at 254 nm (400 mJ/cm^2 followed by 200 mJ/cm^2 UV). After UV cross-linking, neurons were lysed in 1× lysis/immunoprecipitation buffer (1× PXL), and the cross-linked RNA-protein complexes (RNPs) were immunoprecipitated using anti-FUS antibodies (Santa Cruz). RNA 3′ adapters were ligated to the immunoprecipitated RNAs and separated using SDS–PAGE. The gel was transferred onto nitrocellulose membrane and cut the individual lanes between 70 and 100 kDa with a razorblade. Pieces of the membrane were digested in proteinase K to remove the proteins, and purified RNAs were ligated to RNA 5′ adapters. After the reverse transcription reaction and two rounds of PCR, high-throughput sequencing was performed on an Illumina Hiseq2000 (Illumina).

Adapters of CLIP-seq raw sequencing reads were removed using Cutadapt (mentioned before). Reads were mapped to the reference mouse genome (GRCm38/mm10) using Burrows–Wheeler Aligner (v.0.7.17).[28] Peak calling was performed using CLIP Tool Kit.[29] *De novo* motif calling, and peak annotation was performed using software HOMER.[30] Gene Ontology (GO) biological process analysis was performed using MetaScape (mentioned before), visualization of the GO cellular component was achieved using the Cytoscape (v.3.8.2) application ClueGO. Gene network analyses were performed using STRING (http://string-db.org/), clustered using Molecular Complex Detection (MCODE) and visualized in Cytoscape.

Quantitative real-time PCR

The vHPC and mPFC tissues were collected and rapidly transferred into the RNAlater™ Stabilization Solution (Thermo Fisher Scientific). The total RNA was extracted using TRIzol™ (Thermo Fisher Scientific). First-strand cDNA synthesis and amplification were performed by Hifair® III 1st Strand cDNA Synthesis SuperMix for quantitative real-time PCR (qPCR, Yeasen Biotechnology). PCR amplifications were performed using the TB Green® Premix Ex Taq™ II kit (TaKaRa).

Data availability

The experimental data that support findings of this study are available from the corresponding author upon reasonable request.

Results

FUS regulates gene expression and synaptic transmission in a hippocampal subregion-specific manner

Due to embryonic lethal of *Fus* total knockout mouse strain ($Fus^{-/-}$),[31–34] we generated *Fus* conditional knockout mice by crossing $Fus^{fl/fl}$ with Nestin-Cre mice, which eliminates the expression of FUS in neuronal and glial cells from the early developmental stage.[35] The previous studies revealed that the sub-regions of the HPC display distinct gene expression profiles[36,37] and, accordingly, are involved in different biological functions,[38] so we collected HPC from 2-month old Nestin-Cre: $Fus^{fl/fl}$ mice ($n = 3$) and divided them into three sub-regions, i.e. dHPC, iHPC and vHPC, for RNA-seq to gain a deep insight into the functions of FUS in the HPC (Fig. 1A). Each hippocampal sub-region's innate gene expression profile exhibited a pronounced transcriptional heterogeneity across the dorsal–ventral axis, indicating a different transcriptome background in hippocampal sub-regions (Supplementary Fig. 1A). When comparing the differentially expressed genes (DEGs) in each sub-region of the HPC between control and *Fus* KO mice, a total of 2832, 2680 and 1633

DEGs were identified in dHPC, iHPC and vHPC, respectively (Fig. 1B). GO analysis of these DEGs revealed that, although executing physiological roles as one integrative entity, FUS-regulated genes in each sub-region of the HPC are involved in slightly different facets of synaptic functions (Fig. 1C). For example, we notice that the pathways enriched in vHPC are more biased towards cation channel activity. In contrast, those enriched in dHPC are more biased towards postsynaptic functions and the iHPC has overlapping characteristics with both dHPC and vHPC. Nevertheless, Bioinformatics analysis suggests that FUS may participate in establishing sub-region specificity of the HPC, both on gene expression and functional levels. In addition, some well-known FUS-mediated cellular functions were enriched in GO analysis of the 923 overlapping genes, including glutamatergic synapse, RNA metabolic process and localization etc., indicating that our data analysis captured the primary biological functions of FUS (Supplementary Fig. 1B).

To further explore the role of FUS in the adult HPC, we generated Camk2a-Cre; $Fus^{fl/fl}$ mice (hereafter referred to as Fus^{cKO}) by crossing $Fus^{fl/fl}$ mice with Camk2a-Cre mice (Supplementary Fig. 2A), to avoid the functional impairment introduced by FUS deletion at the early development stage.[31–34] Because the expression of Camk2a mRNA starts post-natally and Cre recombinase only expresses in pyramidal neurons of the forebrain (including the HPC and frontal cortex),[39] the resulting Fus^{cKO} mice will specifically delete FUS from pyramidal neurons. The deletion of FUS in the cerebral cortex and HPC was confirmed by western blot and immunofluorescent staining analysis. It is worth pointing out that the protein level of FUS decreased by >50% in mPFC, but there were still many cells, probably inhibitory neurons or other types of cell, expressing FUS (Supplementary Fig. 2B–D).

Our bioinformatics analysis reveals the strong involvement of FUS-regulated genes in synaptic function with some sub-region specificity; further, we investigated whether the FUS region specifically regulates hippocampal synaptic transmission. We therefore recorded mEPSCs of CA1 pyramidal neurons from both the iHPC and vHPC. The Fus^{cKO} indeed showed altered synaptic transmission in both regions. More surprisingly, the regulations are contrary, i.e. while the Fus^{cKO} mice displayed higher mEPSC frequency in the iHPC (Fig. 1D), they had significantly reduced mEPSC frequency in the vHPC (Fig. 1F) compared to the control mice. Combined with the sequencing analysis, these results strongly support that FUS plays a critical role in regulating the excitatory synaptic transmission in a region-specific manner. The amplitude of mEPSCs in both regions remained unaltered in the Fus^{cKO} (Fig. 1E and G), suggesting a presynaptic locus for FUS modulation in iHPC and vHPC.

Loss of FUS in pyramidal neurons leads to FTLD-linked behavioural disinhibition

Dysregulation of the excitatory synaptic transmission in both iHPC and vHPC of the Fus^{cKO} mice suggests these mice may have impaired HPC-mediated cognitive function. The iHPC and vHPC are essential for spatial learning and memory and emotional control, respectively.[40,41] Thus, a series of behavioural tests were run and compared between the control and Fus^{cKO} mice. As indicated by the travel distance in the open field test, the general locomotor activity was unchanged in the Fus^{cKO} mice (Fig. 2A and C). However, these mice showed apparent disruptive avoidance behaviour, evidenced by spending more time in the centre of the open field arena (Fig. 2B), having more entries and staying longer in the open arms during the elevated-plus-maze test (Fig. 2D–F). These findings indicate that the *Fus* conditional knocked-out compromises vHPC-mediated emotional control.

We also evaluated the short- and long-term spatial memory in the Fus^{cKO} mice by Y-maze and Barnes maze. Fus^{cKO} mice had a relatively comparable performance as their control in both tests (Fig. 2G–L), suggesting that lacking *Fus* in the pyramidal neurons does not significantly affect the activities of the iHPC. Additionally, the Fus^{cKO} mice showed normal social interactions (Supplementary Fig. 3A) and social memory (Supplementary Fig. 3B), implying the general integrity of the frontal cortical properties.

Synaptic functions are regulated differently by FUS in disinhibition-related brain regions

vHPC and mPFC are both required for emotional control,[42–45] whose dysfunction directly leads to anxiety or disruptive avoidance behaviours. The Fus^{cKO} mice display a disruptive avoidance behaviour phenotype. To gain insight into the underlying mechanism, we decided to evaluate the detailed neuronal function of FUS in both the vHPC and mPFC (Fig. 3A). Since we have already observed down-regulated excitatory synaptic transmission in the vHPC of the Fus^{cKO} mice, we first examined whether the presynaptic deficit causes this down-regulation by measuring the PPR of the Shaffer Collateral synapses. The Fus^{cKO} mice had much higher PPR when stimulated with 50 Hz (20 ms inter-stimulus interval) paired pulses (Fig. 3B and C), indicative of a reduction in the presynaptic release probability that is in line with the reduced mEPSC frequency. Interestingly, the mEPSCs measured in the mPFC of Fus^{cKO} mice had comparable average frequency (Fig. 3H) and amplitude (Fig. 3I) to those from the control mice, again supporting the brain region-specific modulation by FUS. It is worth noting that the cumulative distributions of the mEPSCs amplitude were not completely overlapping between the Fus^{cKO} and control groups (Fig. 3I, bottom right panel), implying that there might be synapse-specific regulation by FUS in the mPFC. Besides the synaptic alteration, knocking out FUS in both the vHPC and mPFC did not affect the passive membrane properties and the general intrinsic excitability of the pyramidal neurons (Fig. 3E, K and Supplementary Fig. 4). However, the spiking adaptivity altered significantly on large current injection in both regions (Fig. 3F and L). Lacking *Fus* in the vHPC made neurons less adaptive (Fig. 3F), while in the mPFC neurons became more adaptive (Fig. 3L). These opposite changes are probably due to the FUS-mediated reverse modulation of the accommodation of action potential firing in the vHPC and the mPFC (Fig. 3G and M). Our findings unveil the critical physiological function of FUS in regulating synaptic and neuronal properties. Furthermore, the distinct regulatory patterns in the different sub-regions of the HPC and mPFC reveal the complex and region-specific role of FUS.

FUS contributes to disinhibition-related vHPC–mPFC synaptic transmission

The direct synaptic communication between the vHPC and the mPFC is tightly associated with anxiety-like behaviours.[44,45] To examine whether FUS regulates the synaptic transmission of the vHPC–mPFC synapses, we injected AAV virus expressing AAV2/9-hEF1a-DIO-hChR2-EYFP [referred to as ChR2 (Channelrhodopsin-2)], into the ventral CA1 pyramidal neurons of the Fus^{cKO} or Camk2a-Cre mice (Fig. 4A). The brief blue light was used to activate the vHPC axonal terminals, and the light-evoked EPSCs were recorded from layer 2/3 pyramidal neurons in the mPFC (Fig. 4B). Both AMPAR-only and AMPAR/NMDAR-composite currents were evoked by holding cells at –60

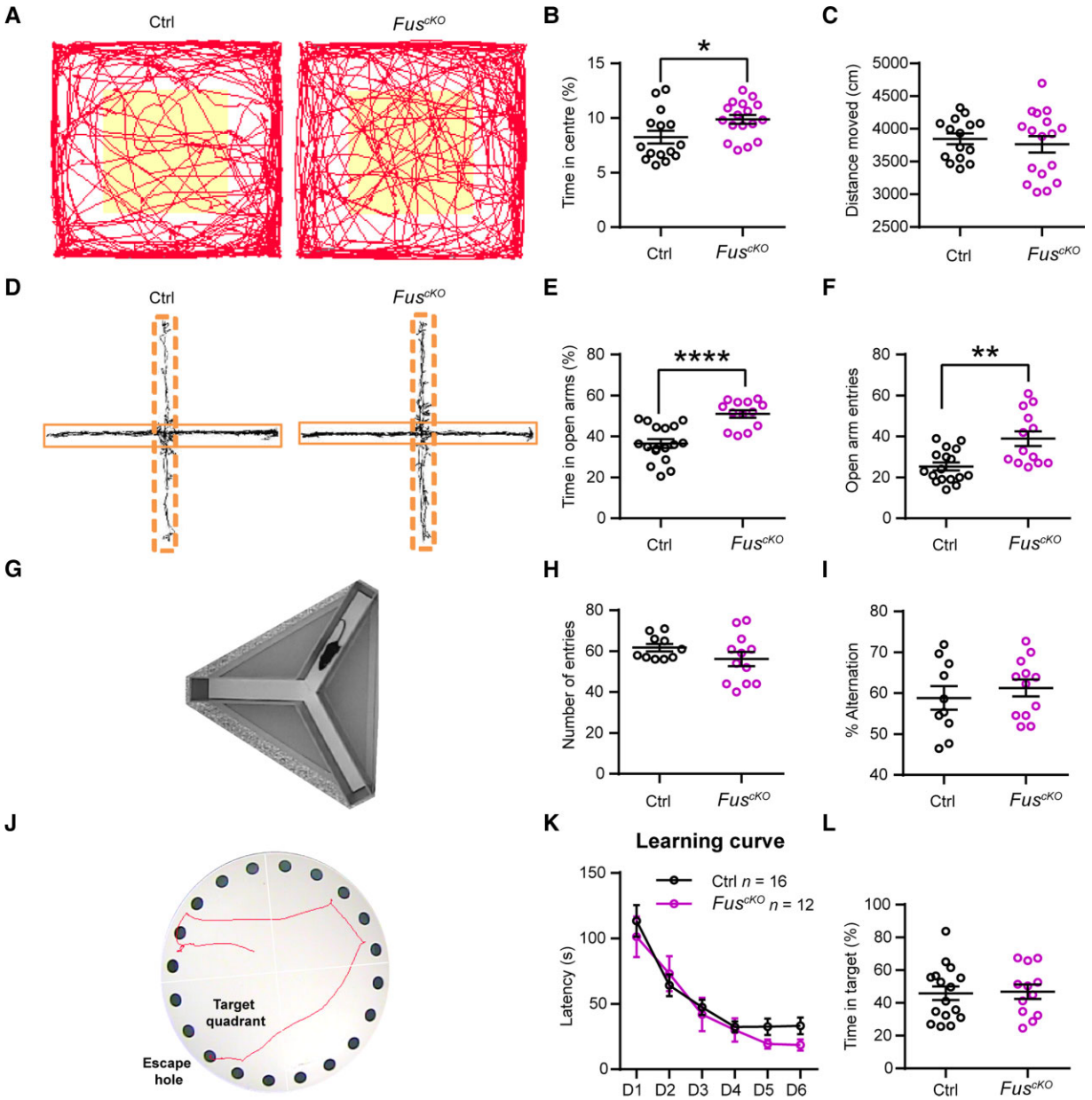

Figure 2 *Fus*^{cKO} mice display FTLD-linked behavioural disinhibition. (**A–C**) Open field test. (**A**) Representative travel traces on the open field test for the Ctrl and *Fus*^{cKO} mice. The yellow shaded part represents the central area. (**B**) *Fus*^{cKO} mice spent more time in the centre of the open field. Student's *t*-test; $^{*}P = 0.026$. (**C**) Distance moved in the open field showed no difference. Student's *t*-test; $P = 0.58$. $n = 15$ Ctrl, $n = 17$ *Fus*^{cKO}. (**D–F**) Elevated-plus maze. (**D**) Representative traces of elevated-plus maze exploration. (**E–F**) *Fus*^{cKO} mice spent significantly more time in the open arms (Student's *t*-test; $^{****}P < 0.0001$) and entered more times in the open arms (Student's *t*-test; $^{**}P = 0.0015$). $n = 17$ Ctrl, $n = 13$ *Fus*^{cKO}. (**G–I**) Y-maze spontaneous alternation test. (**G**) The planform of Y-maze. (**H–I**) No significant difference in performance between groups. (**H**) Summary plot of total arm entries. Student's *t*-test; $P = 0.20$. (**I**) Summary of spontaneous alternation. Student's *t*-test; $P = 0.49$. $n = 10$ Ctrl, $n = 12$ *Fus*^{cKO}. (**J–L**) Barnes maze test. (**J**) Schematic of the Barnes maze. (**K**) Average latencies to the escape hole of two trials per day across six acquisition days for Ctrl and *Fus*^{cKO} mice. No significant difference in learning curve. Two-way ANOVA; $P = 0.21$. (**L**) Time in the target quadrant during the probe trial on day 7. Student's *t*-test; $P = 0.68$. $n = 16$ Ctrl, $n = 12$ *Fus*^{cKO}. Data are presented as the mean ± SEM.

and +40 mV, respectively. The AMPAR/NMDAR was calculated and compared between groups. The *Fus*^{cKO} mice showed a significantly larger AMPAR/NMDAR ratio than the control mice (Fig. 4C), suggesting an altered synaptic transmission in the vHPC–mPFC synapses after knocking out FUS. The increased AMPAR/NMDAR ratio might be caused by an enhanced AMPAR-mediated current and/or a reduced NMDAR-mediated current. To dissect between these possibilities, we first measured the strength of the vHPC synapses onto the mPFC layer 2/3 neurons. The pharmacologically isolated AMPAR EPSCs were recorded after desynchronizing the light-evoked release of vesicles by substituting the extracellular Ca^{2+} with 4 mM Sr^{2+}.[46,47] We then performed the quantal analysis of light-evoked Sr^{2+} desynchronized mEPSCs (Sr^{2+}-mEPSCs, see Materials and Methods), which are mediated by a single vesicle released from the vCA1 terminals. We found that the amplitude of the Sr^{2+}-mEPSCs was increased in the *Fus*^{cKO} mice (Fig. 4D), suggesting that the AMPAR conductance at the vHPC–mPFC synapses are selectively potentiated after knocking out FUS. Interestingly, even though the average AMPAR-mediated

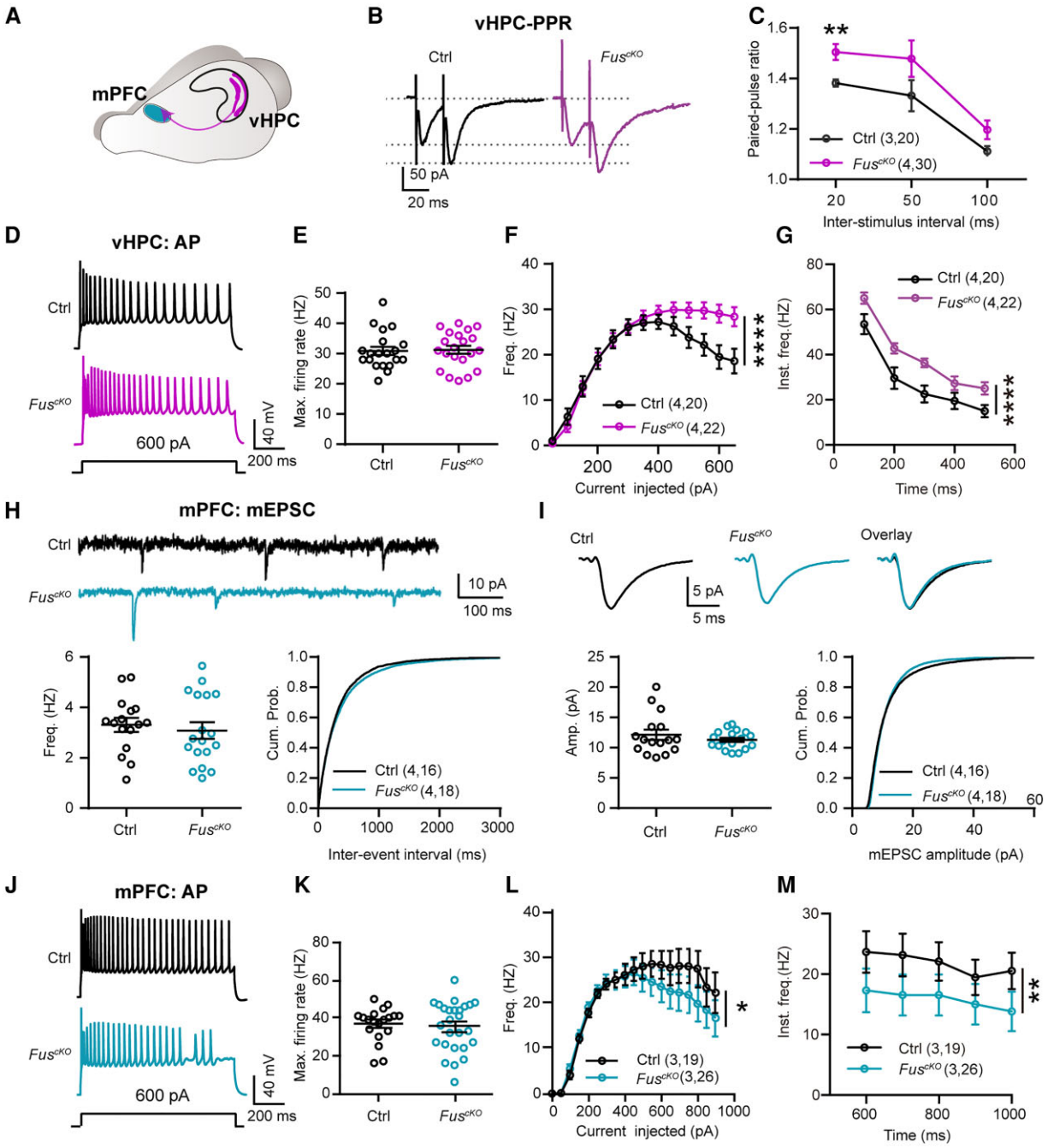

Figure 3 Loss of FUS affects synaptic transmission and neuronal-firing properties of disinhibition-related brain regions. (**A**) vHPC and mPFC are implicated in anxiety-related behaviours in the mice brain. (**B** and **C**) The PPR of evoked EPSCs in Fus^{cKO} mice vHPC was higher than Ctrl mice, especially at the 50 Hz high-frequency stimulation. Paired-pulse stimulations were applied with inter-stimulus intervals of 20, 50 and 100 ms. (**B**) Representative traces of the evoked EPSC at the 20 ms interval. (**C**) Summary graph of PPR at each inter-stimulus interval. Student's *t*-test; 20 ms, $^{**}P = 0.003$; 50 ms, $P = 0.133$; 100 ms, $P = 0.0685$. (**D**–**G**) Knocking out FUS decreased the spike adaptation of vHPC pyramidal neurons. (**D**) Representative traces were recorded by somatically injecting 600 pA currents. (**E**) No significant statistical differences in maximum firing rate between groups. Student's *t*-test; $P = 0.86$. (**F**) Frequency versus injected current for the populations of vHPC pyramidal neurons in Ctrl and Fus^{cKO} mice. Two-way ANOVA test; $^{****}P < 0.0001$. (**G**) The increased instantaneous frequency of spikes in vHPC pyramidal neurons of Fus^{cKO} mice. Two-way ANOVA test; $^{****}P < 0.0001$. (**H**) mEPSC frequency of mPFC pyramidal neurons did not differ between Ctrl and Fus^{cKO} mice. *Top*: Representative traces of mEPSC at mPFC pyramidal neurons in Ctrl and Fus^{cKO} mice. *Bottom left*: Summary of mEPSC frequency in mPFC pyramidal neurons. Student's *t*-test; $P = 0.61$. Bottom right: The distribution of the inter-event intervals showed a slight rightwards shift in Fus^{cKO} mice. KS; $P = 0.0017$. (**I**) mEPSC amplitude and kinetics of mPFC pyramidal neurons did not differ between Ctrl and Fus^{cKO} mice. Top: average traces of well-isolated events. Bottom left: summary of mEPSC amplitude in mPFC pyramidal neurons. Student's *t*-test; $P = 0.34$. *Bottom right*: There was a leftwards shift in the distribution of individual event amplitudes at Fus^{cKO} mice. KS; $P < 0.0001$. (**J**–**M**) Knocking out FUS increased the spike adaptation of vHPC pyramidal neurons. (**J**) Representative traces were recorded by somatically injecting 600 pA currents. (**K**) No significant statistical differences in maximum firing rate between groups. Student's *t*-test; $P = 0.72$. (**L**) Frequency versus injected current for the populations of mPFC pyramidal neurons in Ctrl and Fus^{cKO} mice. Two-way ANOVA test; $^{*}P = 0.0148$. (**M**) The decreased instantaneous frequency of spikes in mPFC pyramidal neurons of Fus^{cKO} mice. Two-way ANOVA test; $^{**}P = 0.0068$. Sample size indicated as (mice, cells). Data are presented as the mean ± SEM.

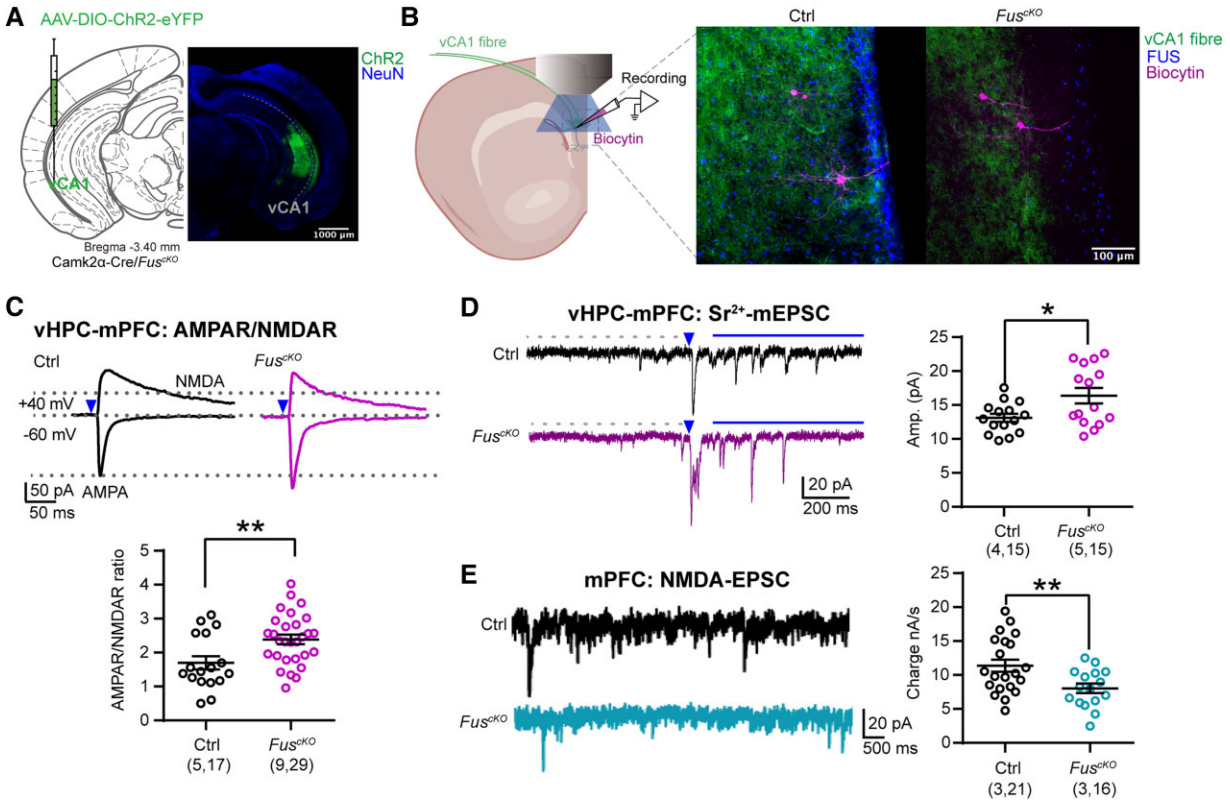

Figure 4 Loss of FUS augments AMPAR-mediated responses of the vHPC–mPFC synapses. (**A**) The representative image of AAV-DIO-ChR2 injection in vCA1 for optogenetic activation of vHPC inputs to mPFC. Green: ChR2; Blue: NeuN. (**B**) *Left*: Schematic showing recording of mPFC responses to optogenetic stimulation of vHPC inputs. Right: representative images are showing the ChR2^{+}-vCA1 fibres, biocytin-labelled neurons and FUS expression in mPFC. Green: vCA1 fibre; Blue: FUS; Magenta: Biocytin. (**C**) FUS knockout increased the AMPAR/NMDAR ratio of vHPC–mPFC synapses. *Top*: Representative traces of light-evoked EPSCs recorded from Ctrl or *Fus*^{cKO} mPFC pyramidal neurons with voltage-clamped at −60 mV (AMPAR EPSC) and +40 mV (NMDAR EPSC). Downwards arrowheads indicate LED stimulation. *Bottom*: Summary plots of AMPAR/NMDAR ratio in Ctrl or *Fus*^{cKO} mPFC pyramidal neurons. Student's *t*-test; $^{**}P = 0.0053$. (**D**) FUS knockout increased light-evoked Sr^{2+}-mEPSC recorded in vHPC–mPFC synapses. *Left*: Representative traces of light-evoked Sr^{2+}-mEPSC recorded from non-ChR2-expressing mPFC pyramidal neurons. LED stimulation was given at the time point indicated with a downwards arrowhead. Light-evoked Sr^{2+}-mEPSC was collected during a time window shown in the solid line. Spontaneous mEPSC was collected during a window before the LED stimulation (dotted line). *Right*: Averaged light-evoked Sr^{2+}-mEPSC amplitude in Ctrl or *Fus*^{cKO} mPFC pyramidal neurons. Student's *t*-test; $^{*}P = 0.016$. (**E**) Decreased NMDAR EPSC of mPFC pyramidal neurons in *Fus*^{cKO} mice. *Left*: Representative traces of NMDAR EPSC were recorded from Ctrl or *Fus*^{cKO} mPFC pyramidal neurons. *Right*: Summary plots of NMDAR EPSC charge. Student's *t*-test; $^{**}P = 0.0088$. Sample size indicated as (mice, cells). Data are presented as the mean ± SEM.

mEPSCs remained unchanged in the mPFC of *Fus*^{cKO} mice, the NMDAR-mediated mEPSCs were significantly reduced (Fig. 4E), which may also contribute to the increased AMPAR/NMDAR ratio at the vHPC–mPFC synapses. Our results imply that FUS synapse specifically modulates the vHPC–mPFC connection, which could be one of the major mechanisms responsible for the disruptive avoidance behaviour of the *Fus*^{cKO} mice.

FUS targets distinct mRNA substrates underlies its brain region-specific regulation of synaptic properties

Previous studies reported that FUS modulates specific RNA targets to affect synapses and neuronal functions.[12,18] To explore whether different RNA targets of FUS participate in regulating neuronal functions of vHPC and mPFC, we first identified possible FUS RNA targets in primary cultured cortical and hippocampal neurons by HITS-CLIP (Fig. 5A, Supplementary Fig. 5A). Bioinformatic analyses revealed that, consistent with the previous studies,[48–51] FUS binds with the introns of its RNA targets predominantly (Supplementary Fig. 5B). GO analysis demonstrated that, functionally, RNA targets of FUS enriched in the synapse organization, modulation of chemical synaptic transmission, behaviour etc. (Fig. 5B, Supplementary Fig. 5C), which is consistent with our RNA-seq data described before. In addition, we also found that many potassium channels (Kcnd2, Kcnq5, Kcnh7) and sodium channels (Scn2a, Scn3a, Scn1b) are binding targets of FUS, which may contribute to the neuronal-firing property changes observed in vHPC and mPFC in *Fus*^{cKO} mice.

We further assessed the protein–protein interactions of the synaptic transmission-related RNA targets of FUS using STRING and Cytoscape (Supplementary Fig. 5D). The MCODE plugin from Cytoscape analysis revealed four subnetworks with high local network connectivity. Notably, the top two of the high interconnection clusters are primarily presynaptic and postsynaptic-related genes (Fig. 5C). Next, we verified these targets by qPCR analysis in vHPC and mPFC of *Fus*^{cKO} mice, respectively, including presynaptic molecules (Rims1, Rims2 and Syt1) and postsynaptic molecules (Gria2, Grin2a and Grin2b) (Fig. 5D, E). The decreased expression of presynaptic genes Rims1, Rims2 and Syt1 may contribute to the decline of presynaptic release we observed in vHPC (Fig. 3C), and two NMDAR subunits Grin2a and Grin2b may contribute to the decline of NMDAR current in mPFC of *Fus*^{cKO} mice (Fig. 4E). Collectively,

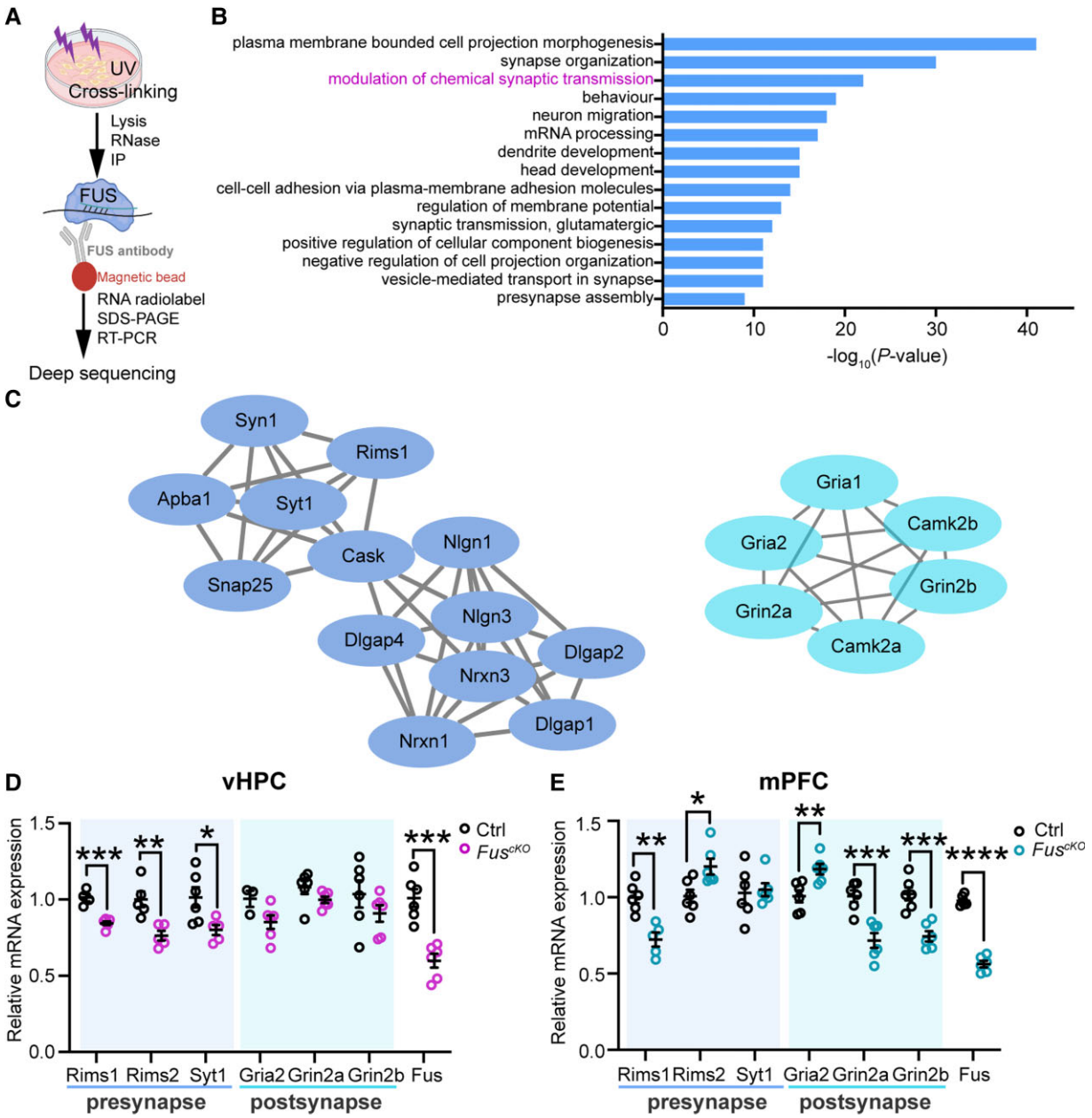

Figure 5 Synaptic transmission-associated gene expression in the vHPC and mPFC are differently regulated by FUS. (**A**) The schematic diagram of the HITS-CLIP. (**B**) Top 15 significant enriched GO biological process of FUS binding targets. (**C**) Top two MCODE clusters derived from the FUS target genes interaction network. (**D** and **E**) Relative mRNA expression level of FUS binding targets in vHPC (**D**) and mPFC (**E**) of Ctrl or Fus^{cKO} mice. $n = 6$ Ctrl, $n = 6$ Fus^{cKO}. Student's *t*-test; $^{*}P < 0.05$, $^{**}P < 0.01$, $^{***}P < 0.001$, $^{****}P < 0.0001$. Data are presented as the mean ± SEM.

these results indicate that FUS targets distinct mRNA substrates underlies its brain region-specific regulation of synaptic properties.

Discussion

FUS is genetically and pathologically associated with ALS and FTLD.[1,2,4,52] Here, we have identified region-specific roles of FUS in regulating transcription and neuronal function in the HPC and mPFC. Strikingly, Fus^{cKO} mice have the selective enhanced synaptic transmission in the vHPC–mPFC synapse, consistent with the mouse's FTLD-linked behavioural disinhibition. Therefore, our study for the first time reveals the region- and synapse-specific physiological role of FUS and sheds light on the molecular and cellular mechanism of the behavioural symptoms associated with FTLD.

Fus^{cKO} mice exhibits disinhibition behaviour

The most pronounced symptoms of behavioural variant FTLD (bvFTLD) include changes in personality, interpersonal conduct, emotional modulation and progressive disintegration of the neural circuits involved in social cognition, emotion regulation, motivation and decision making.[6,53,54] FTLD-FUS cases are relatively early onset and have negative family history, severe caudate atrophy on MRI[55–57] and bvFTLD symptoms. Emerging evidence indicates that FUS mutations incur gain-of toxicity to drive ALS

pathogenesis[10,11,13,31,58,59]; however, cases of FTLD-FUS tend to be sporadic, with rare cases associated with genetic inheritance.[5,60–62] In this study, we observed the impairment of synaptic transmission and disinhibition in anxiety-like behaviour as early as 2 months of age, which agrees with the early onset of FTLD-FUS. Behaviour analysis in Fus^{cKO} mice revealed a disruptive avoidance behaviour, normal spatial learning and memory, and locomotion activity, which partially recapitulate bvFTLD phenotypes.[6,63,64] The disruptive avoidance behaviour has also been previously documented in other FUS knockout mouse models.[18,34] However, the normal locomotive activity of our Fus^{cKO} mice can rule out other behaviour changes caused by locomotion changes.

FUS regulates synaptic transmission in a region-specific manner

Neurodegenerative diseases usually show region-specific pathology.[54,65] In post-mortem brain sections of FTLD-FUS cases, FUS immunoreactivity is observed in the cerebral neocortex, HPC and some subcortical regions[8]; consistently, we found that FUS plays diverse roles depending on the cell location and synaptic connections by comparing transcriptome, synaptic transmission, neuronal properties and brain region-associated behaviours. Our findings are in line with a previous study showing similar region- and cell type-specific transcriptomic regulation by FUS in primary cell cultures.[66] Opposite changes in firing properties of vHPC and mPFC pyramidal neurons may disrupt the synchronization between vHPC and mPFC, which is proposed as an essential mechanism underlying the anxiety-like avoidance behaviour.[45] The unique enhancement of the vHPC–mPFC synapses further suggests that the lack of FUS function may accounts for the progressive disintegration of the neural circuits in bvFTLD.[54,67] Therefore, our findings provide a potential explanation for the brain region- and function-selective vulnerability in FTLD-FUS.[21,68]

FUS regulates the expression of many synaptic transmission and plasticity-related genes

As an RNA-binding protein, numerous RNA targets of FUS have been identified so far[49,50,69,70]; many are involved in synaptic transmission and plasticity.[12,18,70] In this study, we identified and confirmed the expressions of some pre- and postsynaptic targets of FUS in vHPC and mPFC, including Rims1, Rims2 and Syt1 in vHPC, and Grin2a, Grin2b in mPFC, which may underlie the decreased presynaptic release probability in vHPC, and the decreased NMDAR response in mPFC, respectively. The recent CLIP-seq data on cortical synaptoneurosomes also revealed the binding of FUS with Syt1 and Gria2 at the synapse,[70] which further implies the diversity of synaptic modulation by FUS.

In summary, we report in this study that FUS regulates synaptic function in a region-specific manner, and FUS-mediated synaptic transmission from vHPC to mPFC plays a critical role in FTLD-linked disinhibition. Our study provides a mechanistic explanation for the emotional deficits of FTLD and expands our understanding of FTLD pathology.

Acknowledgements

We thank Dr Xing-Qun Liang of Tongji University and Dr Xiao-Han Wang for critical reading of the manuscript. All members of the Wang and He laboratory for the discussions and suggestions. We thank the staff members of the Animal Facility at the National Facility for Protein Science in Shanghai (NFPS), Shanghai Advanced Research Institute, Chinese Academy of Sciences, China for providing technical support and assistance in data collection and analysis.

Funding

This work is supported by The National Key Research and Development Program (2018YFA0107903), National Natural Science Foundation (31471018, 31671055, 31700917, 32070963) and Shanghai Municipal Science and Technology Major Project (2019SHZDZX02), and Shanghai Science and Technology Development Funds (22ZR1475100).

Competing interests

The authors declare no competing interests.

Supplementary material

Supplementary material is available at Brain online.

References

1. Kwiatkowski TJ Jr, Bosco DA, Leclerc AL, *et al*. Mutations in the FUS/TLS gene on chromosome 16 cause familial amyotrophic lateral sclerosis. *Science*. 2009;323:1205-1208.
2. Vance C, Rogelj B, Hortobagyi T, *et al*. Mutations in FUS, an RNA processing protein, cause familial amyotrophic lateral sclerosis type 6. *Science*. 2009;323:1208-1211.
3. Deng H, Gao K, Jankovic J. The role of FUS gene variants in neurodegenerative diseases. *Nat Rev Neurol*. 2014;10:337-348.
4. Broustal O, Camuzat A, Guillot-Noel L, *et al*. FUS mutations in frontotemporal lobar degeneration with amyotrophic lateral sclerosis. *J Alzheimers Dis*. 2010;22:765-769.
5. Van Langenhove T, van der Zee J, Sleegers K, *et al*. Genetic contribution of FUS to frontotemporal lobar degeneration. *Neurology*. 2010;74:366-371.
6. Bang J, Spina S, Miller BL. Frontotemporal dementia. *Lancet*. 2015;386:1672-1682.
7. Ling SC, Polymenidou M, Cleveland DW. Converging mechanisms in ALS and FTD: Disrupted RNA and protein homeostasis. *Neuron*. 2013;79:416-438.
8. Mackenzie IR, Munoz DG, Kusaka H, *et al*. Distinct pathological subtypes of FTLD-FUS. *Acta Neuropathol*. 2011;121:207-218.
9. Huang C, Tong J, Bi F, *et al*. Entorhinal cortical neurons are the primary targets of FUS mislocalization and ubiquitin aggregation in FUS transgenic rats. *Hum Mol Genet*. 2012;21:4602-4614.
10. Sephton CF, Tang AA, Kulkarni A, *et al*. Activity-dependent FUS dysregulation disrupts synaptic homeostasis. *Proc Natl Acad Sci U S A*. 2014;111:E4769-E4778.
11. Qiu H, Lee S, Shang Y, *et al*. ALS-associated mutation FUS-R521C causes DNA damage and RNA splicing defects. *J Clin Invest*. 2014;124:981-999.
12. Yokoi S, Udagawa T, Fujioka Y, *et al*. 3' UTR length-dependent control of SynGAP isoform alpha2 mRNA by FUS and ELAV-like proteins promotes dendritic spine maturation and cognitive function. *Cell Rep*. 2017;20:3071-3084.
13. Lopez-Erauskin J, Tadokoro T, Baughn MW, *et al*. ALS/FTD-linked mutation in FUS suppresses intra-axonal protein synthesis and drives disease without nuclear loss-of-function of FUS. *Neuron*. 2020;106:354.

14. Fujii R, Takumi T. TLS facilitates transport of mRNA encoding an actin-stabilizing protein to dendritic spines. *J Cell Sci*. 2005; 118:5755-5765.
15. Aoki N, Higashi S, Kawakami I, *et al*. Localization of fused in sarcoma (FUS) protein to the post-synaptic density in the brain. *Acta Neuropathol*. 2012;124:383-394.
16. Armstrong GA, Drapeau P. Loss and gain of FUS function impair neuromuscular synaptic transmission in a genetic model of ALS. *Hum Mol Genet*. 2013;22:4282-4292.
17. Machamer JB, Collins SE, Lloyd TE. The ALS gene FUS regulates synaptic transmission at the *Drosophila* neuromuscular junction. *Hum Mol Genet*. 2014;23:3810-3822.
18. Udagawa T, Fujioka Y, Tanaka M, *et al*. FUS regulates AMPA receptor function and FTLD/ALS-associated behaviour via GluA1 mRNA stabilization. *Nat Commun*. 2015;6:7098.
19. Verfaillie SC, Adriaanse SM, Binnewijzend MA, *et al*. Cerebral perfusion and glucose metabolism in Alzheimer's disease and frontotemporal dementia: Two sides of the same coin? *Eur Radiol*. 2015;25:3050-3059.
20. Bertoux M, Volle E, de Souza LC, Funkiewiez A, Dubois B, Habert MO. Neural correlates of the mini-SEA (social cognition and emotional assessment) in behavioral variant frontotemporal dementia. *Brain Imaging Behav*. 2014;8:1-6.
21. Laakso MP, Frisoni GB, Kononen M, *et al*. Hippocampus and entorhinal cortex in frontotemporal dementia and Alzheimer's disease: A morphometric MRI study. *Biol Psychiatry*. 2000;47:1056-1063.
22. Martin M. Cutadapt removes adapter sequences from high-throughput sequencing reads. *EMBnet J*. 2011;17:10-12.
23. Pertea M, Kim D, Pertea GM, Leek JT, Salzberg SL. Transcript-level expression analysis of RNA-seq experiments with HISAT, StringTie and ballgown. *Nat Protoc*. 2016;11:1650-1667.
24. Liao Y, Smyth GK, Shi W. Featurecounts: An efficient general purpose program for assigning sequence reads to genomic features. *Bioinformatics*. 2014;30:923-930.
25. Love MI, Huber W, Anders S. Moderated estimation of fold change and dispersion for RNA-seq data with DESeq2. *Genome Biol*. 2014;15:550.
26. Zhou Y, Zhou B, Pache L, *et al*. Metascape provides a biologist-oriented resource for the analysis of systems-level datasets. *Nat Commun*. 2019;10:1523.
27. Moore MJ, Zhang C, Gantman EC, Mele A, Darnell JC, Darnell RB. Mapping argonaute and conventional RNA-binding protein interactions with RNA at single-nucleotide resolution using HITS-CLIP and CIMS analysis. *Nat Protoc*. 2014;9:263-293.
28. Li H, Durbin R. Fast and accurate short read alignment with Burrows-Wheeler transform. *Bioinformatics*. 2009;25:1754-1760.
29. Shah A, Qian Y, Weyn-Vanhentenryck SM, Zhang C. CLIP Tool kit (CTK): A flexible and robust pipeline to analyze CLIP sequencing data. *Bioinformatics*. 2017;33:566-567.
30. Heinz S, Benner C, Spann N, *et al*. Simple combinations of lineage-determining transcription factors prime cis-regulatory elements required for macrophage and B cell identities. *Mol Cell*. 2010;38:576-589.
31. Scekic-Zahirovic J, Sendscheid O, El Oussini H, *et al*. Toxic gain of function from mutant FUS protein is crucial to trigger cell autonomous motor neuron loss. *EMBO J*. 2016;35:1077-1097.
32. Hicks GG, Singh N, Nashabi A, *et al*. FUS deficiency in mice results in defective B-lymphocyte development and activation, high levels of chromosomal instability and perinatal death. *Nat Genet*. 2000;24:175-179.
33. Kuroda M, Sok J, Webb L, *et al*. Male sterility and enhanced radiation sensitivity in $TLS^{(-/-)}$ mice. *EMBO J*. 2000;19:453-462.
34. Kino Y, Washizu C, Kurosawa M, *et al*. FUS/TLS deficiency causes behavioral and pathological abnormalities distinct from amyotrophic lateral sclerosis. *Acta Neuropathol Commun*. 2015;3:24.
35. Zimmerman L, Parr B, Lendahl U, *et al*. Independent regulatory elements in the nestin gene direct transgene expression to neural stem cells or muscle precursors. *Neuron*. 1994;12:11-24.
36. Cembrowski MS, Bachman JL, Wang L, Sugino K, Shields BC, Spruston N. Spatial gene-expression gradients underlie prominent heterogeneity of CA1 pyramidal neurons. *Neuron*. 2016; 89:351-368.
37. Cembrowski MS, Wang L, Sugino K, Shields BC, Spruston N. Hipposeq: A comprehensive RNA-seq database of gene expression in hippocampal principal neurons. *eLife*. 2016;5:e14997.
38. Bannerman DM, Sprengel R, Sanderson DJ, *et al*. Hippocampal synaptic plasticity, spatial memory and anxiety. *Nat Rev Neurosci*. 2014;15:181-192.
39. Tsien JZ, Chen DF, Gerber D, *et al*. Subregion- and cell type-restricted gene knockout in mouse brain. *Cell*. 1996;87: 1317-1326.
40. Jeffery KJ. The hippocampus: From memory, to map, to memory map. *Trends Neurosci*. 2018;41:64-66.
41. Calhoon GG, Tye KM. Resolving the neural circuits of anxiety. *Nat Neurosci*. 2015;18:1394-1404.
42. Kjelstrup KG, Tuvnes FA, Steffenach HA, Murison R, Moser EI, Moser MB. Reduced fear expression after lesions of the ventral hippocampus. *Proc Natl Acad Sci U S A*. 2002;99:10825-10830.
43. Shah AA, Treit D. Excitotoxic lesions of the medial prefrontal cortex attenuate fear responses in the elevated-plus maze, social interaction and shock probe burying tests. *Brain Res*. 2003; 969:183-194.
44. Padilla-Coreano N, Bolkan SS, Pierce GM, *et al*. Direct ventral hippocampal-prefrontal input is required for anxiety-related neural activity and behavior. *Neuron*. 2016;89:857-866.
45. Padilla-Coreano N, Canetta S, Mikofsky RM, *et al*. Hippocampal-prefrontal theta transmission regulates avoidance behavior. *Neuron*. 2019;104:601-610 e4.
46. Gil Z, Connors BW, Amitai Y. Efficacy of thalamocortical and intracortical synaptic connections: Quanta, innervation, and reliability. *Neuron*. 1999;23:385-397.
47. Petrus E, Isaiah A, Jones AP, *et al*. Crossmodal induction of thalamocortical potentiation leads to enhanced information processing in the auditory cortex. *Neuron*. 2014;81:664-673.
48. Hoell JI, Larsson E, Runge S, *et al*. RNA Targets of wild-type and mutant FET family proteins. *Nat Struct Mol Biol*. 2011;18:1428-1431.
49. Ishigaki S, Masuda A, Fujioka Y, *et al*. Position-dependent FUS-RNA interactions regulate alternative splicing events and transcriptions. *Sci Rep*. 2012;2:529.
50. Lagier-Tourenne C, Polymenidou M, Hutt KR, *et al*. Divergent roles of ALS-linked proteins FUS/TLS and TDP-43 intersect in processing long pre-mRNAs. *Nat Neurosci*. 2012;15:1488-1497.
51. Nakaya T, Alexiou P, Maragkakis M, Chang A, Mourelatos Z. FUS regulates genes coding for RNA-binding proteins in neurons by binding to their highly conserved introns. *RNA*. 2013;19:498-509.
52. Deng HX, Zhai H, Bigio EH, *et al*. FUS-immunoreactive inclusions are a common feature in sporadic and non-SOD1 familial amyotrophic lateral sclerosis. *Ann Neurol*. 2010;67:739-748.
53. Piguet O, Hornberger M, Mioshi E, Hodges JR. Behavioural-variant frontotemporal dementia: Diagnosis, clinical staging, and management. *Lancet Neurol*. 2011;10:162-172.
54. Seeley WW. Selective functional, regional, and neuronal vulnerability in frontotemporal dementia. *Curr Opin Neurol*. 2008; 21:701-707.
55. Loy CT, McCusker E, Kril JJ, *et al*. Very early-onset frontotemporal dementia with no family history predicts underlying fused in sarcoma pathology. *Brain*. 2010;133:e158-e159.

56. Seelaar H, Klijnsma KY, de Koning I, *et al*. Frequency of ubiquitin and FUS-positive, TDP-43-negative frontotemporal lobar degeneration. *J Neurol*. 2010;257:747-753.
57. Josephs KA, Whitwell JL, Parisi JE, *et al*. Caudate atrophy on MRI is a characteristic feature of FTLD-FUS. *Eur J Neurol*. 2010;17: 969-975.
58. Sharma A, Lyashchenko AK, Lu L, *et al*. ALS-associated mutant FUS induces selective motor neuron degeneration through toxic gain of function. *Nat Commun*. 2016;7:10465.
59. Ling SC, Dastidar SG, Tokunaga S, *et al*. Overriding FUS autoregulation in mice triggers gain-of-toxic dysfunctions in RNA metabolism and autophagy-lysosome axis. *eLife*. 2019;8:e40811.
60. Mackenzie IR, Rademakers R, Neumann M. TDP-43 and FUS in amyotrophic lateral sclerosis and frontotemporal dementia. *Lancet Neurol*. 2010;9:995-1007.
61. Huey ED, Ferrari R, Moreno JH, *et al*. FUS And TDP43 genetic variability in FTD and CBS. *Neurobiol Aging*. 2012;33:1016 e9-1016 e17.
62. Snowden JS, Hu Q, Rollinson S, *et al*. The most common type of FTLD-FUS (aFTLD-U) is associated with a distinct clinical form of frontotemporal dementia but is not related to mutations in the FUS gene. *Acta Neuropathol*. 2011;122:99-110.
63. Hodges JR, Patterson K, Ward R, *et al*. The differentiation of semantic dementia and frontal lobe dementia (temporal and frontal variants of frontotemporal dementia) from early Alzheimer's disease: A comparative neuropsychological study. *Neuropsychology*. 1999;13:31-40.
64. Seelaar H, Rohrer JD, Pijnenburg YA, Fox NC, van Swieten JC. Clinical, genetic and pathological heterogeneity of frontotemporal dementia: A review. *J Neurol Neurosurg Psychiatry*. 2011; 82:476-486.
65. Pandya VA, Patani R. Region-specific vulnerability in neurodegeneration: Lessons from normal ageing. *Ageing Res Rev*. 2021; 67:101311.
66. Fujioka Y, Ishigaki S, Masuda A, *et al*. FUS-regulated region- and cell-type-specific transcriptome is associated with cell selectivity in ALS/FTLD. *Sci Rep*. 2013;3:2388.
67. Seeley WW, Crawford RK, Zhou J, Miller BL, Greicius MD. Neurodegenerative diseases target large-scale human brain networks. *Neuron*. 2009;62:42-52.
68. Vogel JW, La Joie R, Grothe MJ, *et al*. A molecular gradient along the longitudinal axis of the human hippocampus informs large-scale behavioral systems. *Nat Commun*. 2020;11:1-17.
69. Rogelj B, Easton LE, Bogu GK, *et al*. Widespread binding of FUS along nascent RNA regulates alternative splicing in the brain. *Sci Rep*. 2012;2:603.
70. Sahadevan S, Hembach KM, Tantardini E, *et al*. Synaptic FUS accumulation triggers early misregulation of synaptic RNAs in a mouse model of ALS. *Nat Commun*. 2021;12:3027.